Available online at www.sciencedirect.com

ScienceDirect

Energy Procedia 129 (2017) 716–723

Energy Procedia

www.elsevier.com/locate/procedia

IV International Seminar on ORC Power Systems, ORC2017
13-15 September 2017, Milano, Italy

Thermodynamic comparison and dynamic simulation of direct and indirect solar organic Rankine cycle systems with PCM storage

Jahan Zeb Alvi[a], Muhammad Imran[b], Gang Pei[a]*, Jing Li[a], Guangtao Gao[a], Junaid Alvi[c]

[a]*Department of Thermal Science and Energy Engineering, University of Science and Technology of China, Hefei, Anhui, China*
[b]*University of Management and Technology, Lahore, Pakistan*
[c]*Key Laboratory of Efficient Utilization of Low and Medium Grade Energy, MOE, School of Mechanical Engineering, Tianjin University, Tianjin 300072, China*

Abstract

A thermodynamic comparison between a novel direct solar ORC system (DSOS) and indirect solar ORC system (ISOS) is carried out in this study. A phase change material (PCM) heat storage unit is integrated with both systems to ensure the stability of power generation. Water and R245fa are selected as a heat transfer fluids (HTFs) for ISOS and DSOS respectively. However, R245fa is used as working fluid for both systems. Weekly, monthly and annual dynamic simulations are carried out to compare the performance of both systems using hourly weather data of Islamabad, Pakistan. ISOS has shown 1.71% system efficiency and able to provide 34.02 kW/day power while DSOS has shown 4.5 times higher system efficiency and 2.8 times higher power on annual basis. Numerical model for the PCM storage is developed and validated with the previous experimental data. Average annual amount of energy stored by PCM during charging phase for ISOS is 4.24 MW/day higher than DSOS. However, in comparison with ISOS, DSOS has delivered 33.80 kW/day more power to HTF during discharging phase of the PCM on annual basis. Maximum benefits of PCM storage are observed during the summer season compared to the winter season at selected operating conditions. Furthermore, average annual increment in capacity factor by using PCM storage are found to be 21.71% and 17% for DSOS and ISOS respectively.

Peer-review under responsibility of the scientific committee of the IV International Seminar on ORC Power Systems.

Keywords: ISOS; DSOS; PCM storage;Capacity factor

* Corresponding author. Tel.: +86 551 3601641
E-mail address: peigang@ustc.edu.cn

1876-6102
Peer-review under responsibility of the scientific committee of the IV International Seminar on ORC Power Systems.
10.1016/j.egypro.2017.09.103

1. Thermodynamic modelling

Schematic diagram of both systems are shown in Figure 1 and 2, respectively. In case of DSOS as shown in Figure 1, evaporator is replaced by solar collector in charging mode. However, PCM storage tank work as evaporator during discharging mode. R245fa is used as working fluid as well as a HTF in the system. One variable flow pump namely P_1 is used to regulate the flow of fluid within the system. In case of ISOS, water is selected as HTF in solar loop while R245fa is used as working fluid ORC loop as shown in Figure 2. Two variable flow pumps namely P_1 and P_2 are used to regulate the HTF & working fluid in solar loop and ORC loop respectively. Five flow control valves are employed to control the fluid flow in both systems. These valves may open and close depending upon the operating and boundary conditions which are discussed in details in section below

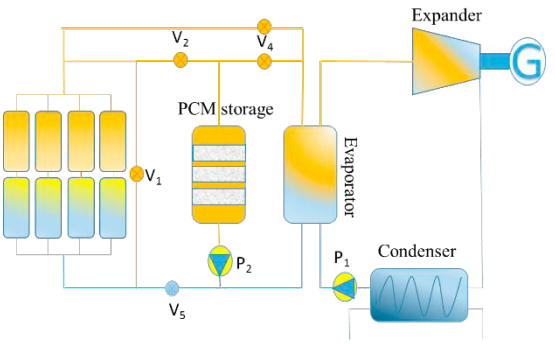

Figure 1. Layout diagram of ISOS

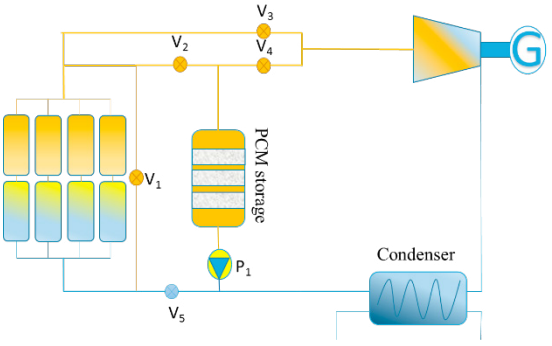

Figure 2. Layout diagram of DSOS

1.1. Solar radiations received at collector surface

Solar radiations received by tilted surface of the EFPC are calculated by

$$I_t = \left(I_b + I_d \frac{I_b}{I_h} \right) R_b + I_d \left(1 - \frac{I_b}{I_h} \right) \left(\frac{1+\cos\beta}{2} \right) \left(1 + \sqrt{\frac{I_b}{I_h}} \mathrm{Sin}^3 \left(\frac{\beta}{2} \right) \right) + I_h \rho_g \left(\frac{1-\cos\beta}{2} \right) \tag{1}$$

Where I_b, I_d, I_h, R_b, ρ_g and β are the direct beam, diffuse beam, sum of direct and diffuse beam, ratio of total radiation on titled surface to that on the horizontal surface, surface angle (collector angle) and reflectance from the surroundings [1].

1.2. Efficiency of Solar colector array

Solar collector efficiency is calculated as a function of collector inlet temperature, the ambient air temperature and total solar radiations received at collector surface

$$\eta_{cl} = a_0 - a_1 \frac{(T_i - T_{amb})}{I_t} - a_2 \frac{(T_i - T_{amb})^2}{I_t} \tag{2}$$

Where a_0, a_1, a_2, T_i and T_{amb} are optical efficiency of the collector, linear heat loss coefficient, quadratic heat loss coefficient, the inlet and ambient temperatures respectively[2]. It is assumed that each collector array consist of 75 collectors each solar collector have a size of 2 m^2. Amount of heat absorbed by the solar collectors array is calculated by

$$q_{cl} = \eta_{cl} \times I_t \times n \times A_{cl} \tag{3}$$

Where q_{cl}, n and A_{cl} are the amount of heat absorbed by collectors, the number of solar collectors and area of a solar collector respectively. Outlet temperature at the solar collector array is calculated by

$$T_o = T_i + \left(\frac{q_{cl}}{\left(m_f C_p \right)} \right) \tag{4}$$

Where T_o, m_f and C_p are the outlet temperature at solar collectors array, mass flow rate of heat transfer fluid and specific heat capacity of the fluid respectively.

1.3. Phase change material storage

The typical configurations of the PCM storage is shown in Figures. A cylindrical storage tank is considered. It contains a coiled shape pipe containing heat transfer fluid passing through PCM filled tank. Charging and discharging process are simulated on the basis of heat transfer fluid for both systems. During chagrining process, the temperature of PCM rises in solid phase until it reaches up to the melting point of PCM. After this point, temperature remains constant during the melting process. After phase change process is completed and all of the PCM turns into liquid phase, the temperature of the liquid PCM rises up to the limit imposed by HTF. However, during discharging process, thermal energy stored by liquid PCM is removed by cold HTF[3]. The governing equations for HTF and PCM are based on the model well known enthalpy model given by equation (5).

Following are the assumptions that have been used while solving the enthalpy method to calculate the heat transfer in PCM.

- Conduction is considered as dominant heat transfer mechanism within the PCM
- One dimensional heat transfer is considered at this stage.
- Sub cooling of the PCM that may not be a dominant factor in paraffinic PCMs is not considered.
- Natural convection which may occur due to the density difference in the PCM is not considered in the current model [4].

$$\rho \frac{\partial H}{\partial t} = \kappa_{pcm} \frac{\partial^2 T_{pcm}}{\partial y^2} \tag{5}$$

In equation (5), the total volumetric enthalpy "H" includes the latent heat of the PCM along with the sensible energy of PCM at a given temperature. Therefore, the total volumetric enthalpy of PCM at any given temperature is calculated using the following relation

$$H = \begin{cases} \rho_{pcm}.C_{pcm}(T_{pcm} - T_m) & for \quad T_{pcm} < T_m \quad Solid\,region \\ \rho_{pcm}.C_{pcm}(T_{pcm} - T_m) + \lambda.\rho_{pcm} & for \quad T_{pcm} > T_m \quad Liguid\,region \end{cases} \tag{6}$$

From equation (6), if PCM is in solid phase, latent heat of the material is zero and it only contains sensible heat. In liquid phase, total volumetric enthalpy is the combination of latent heat and sensible heat where Tm is the melting point of PCM. Temperature of the PCM "T_{pcm}" is calculated from the volumetric enthalpy of the PCM using the following relations

$$T_{pcm} = \begin{cases} T_m + \dfrac{H}{\rho_{pcm}.C_{pcm}} & for \quad H < 0 \\ T_m & for \quad 0 < H < \rho_{pcm}.\lambda \\ T_m + \dfrac{H - (\rho_{pcm}.\lambda)}{\rho_{pcm}.C_{pcm}} & for \quad H > \rho_{pcm}.\lambda \end{cases} \tag{7}$$

Thermo-physical properties of PCM is given in table1 and design parameters of ORC are shown in table 2.

Table 1. Thermo-physical properties of PCM

Commercial Name	Salt hydrate
PCM category	inorganic
Melting point	117ºC
Latent heat	160 kJ/kg
Specific heat capacity	2.61 kJ/kg-K

Table 2. Design parameters of ORC

Parameter	Value
HTF mass flow rate in kg/s	0.5
Pinch point temperature difference in evaporator and condenser	10 ºC
Turbine efficiency for initial cycle design	80%
Pump efficiency for initial cycle design	60%
Degree of superheating at turbine inlet	3 ºC

Amount of energy stored by PCM during charging mode is calculated by difference in latent heat between final and initial node of PCM storage tank.

$$Q_{st,c} = M_{pcm}(\lambda_{\mathrm{mx}} - \lambda_{in}) \tag{8}$$

Power transferred to HTF during discharging mode is calculated by equation (9)

$$P_{tr,d} = m_{HTF} C_{HTF} (T_{HTF,o} - T_{HTF,i}) \tag{9}$$

1.4. ORC modelling

The basic Organic Rankine Cycle (ORC) configuration has been chosen for the simulation study due to lower capital investment for low-medium temperature applications. The operating conditions and assumptions for the design of the ORC system are listed in the below sections.

The isentropic efficiency for the expander and the pump is defined by Eq. (10) and Eq. (11)

$$\varepsilon_t = \frac{h_{t,i} - h_{t,o}}{h_{t,i} - h_{t,os}} \tag{10}$$

$$\varepsilon_p = \frac{h_{p,os} - h_{p,i}}{h_{p,o} - h_{p,i}} \tag{11}$$

Where os represents the ideal thermodynamic process. The energy required in the heating process of the ORC is calculated by the enthalpy increment of the organic fluid from the pump to the expander.

$$W_{net} = W_t \varepsilon_g - W_p \tag{12}$$

$$Q_{ORC} = m_{wf}\left(h_{t,i} - h_{p,o}\right) \tag{13}$$

The ORC efficiency is defined by the ratio of the net power output to the heat supplied [5].

$$\eta_{ORC} = \frac{W_{net}}{Q_{ORC}} \tag{14}$$

The overall electricity efficiency of the solar ORC is expressed by

$$\eta_{sys} = \eta_{ORC}.\eta_{cl} \tag{15}$$

Increment in capacity factor of the systems is calculated by relative increment in working hours by use of PCM storage.

$$CF_{inc} = \frac{Wh_{\mathrm{w,pcm}} - Wh_{wo,pcm}}{Wh_{\mathrm{w,pcm}}} \tag{16}$$

1.5. Operating and boundary conditions

Each component in both systems is controlled and turned on and off by logical functions depending on several simulation parameters, hence implementing the desired system control logic. The operation modes of storage system are divided into charging and discharging mode. The initial temperature of PCM is selected to be 373.15 K. This depicts that PCM is in solid phase at the beginning of simulation process. The values of TMY data for the Islamabad is imported in MATLAB from the metronome software. Same operating and boundary condition are applied to both systems. The minimum threshold level of solar radiation received at the surface of collector, at which system starts working, is selected to be 400 W/m2 otherwise system stops or undergoes to discharging process. The PCM storage system is designed to work at melting point temperature of the PCM. It means that largest part of charging and discharging process occurs at melting point temperature. Therefore, maximum temperature at the outlet of collector array is selected to be 390 K. HTF mass flow rate across PCM storage tank is increased with increase in temperature over the limit imposed.

2. Results, Analysis and Discussions

In this section, Thermodynamic comparison between ISOS and DSOS is carried out. Weekly simulations have been done for hottest and coldest week of the year. Hourly average daily system efficiency, net power output, temperature variation at each hour across PCM storage tank during charging phase and hourly average temperature variation across each node during discharging phase are calculated for both systems. Moreover, Monthly average yearly system efficiency, net power, amount of energy stored by PCM storage during charging mode and power transferred to HTF during discharging mode are computed for both systems. Furthermore, increment in capacity factor by use of PCM storage is calculated and results are compared for both systems.

2.1. Performance during hottest week of the year

2.1.1. Charging mode of PCM storage

Figure 3 & 4 shows ISOS and DSOS hourly average daily temperature of PCM and HTF during charging mode for hottest week (2nd week of June) respectively. Number of charging hours for ISOS and DSOS are observed to be 8 and 7 hours respectively. In case of ISOS, rise in average temperature PCM storage tank is observed to be 7.7 ^{o}C. However, in case of DSOS, this value reaches up to 18.5 ^{o}C. At maximum HTF temperature, the temperature difference between HTF and PCM are found to be 10 ^{o}C and 0 ^{o}C for ISOS and DSOS respectively. Therefore, it depicts DSOS has shown stronger thermal match between HTF and PCM as compared to ISOS.

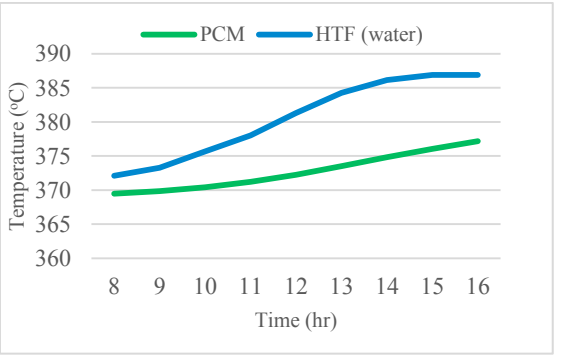

Figure 3. PCM and HTF temperature for ISOS

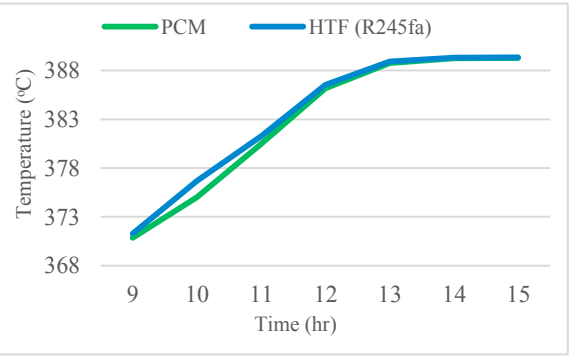

Figure 4. PCM and HTF temperature for DSOS

Furthermore, at selected operating and boundary conditions, HTF temperature of DSOS increases sharply and reaches up to PCM melting point temperature. However, in case of ISOS, operating temperature cannot reach to that

point. Reason behind this phenomena is that, at the given temperature range, specific heat of R245fa is almost 2.5 times lower than water. Therefore, temperature rise sharply for DSOS.

2.1.2. Discharging mode of PCM

PCM storage tank is divided into 105 equally spaced nodes. Temperature at each node is calculated for every hour during simulation process. Figure 5 & 6 depicts ISOS and DSOS hourly average variation in temperature of PCM and HTF across the PCM storage tank during discharging mode for hottest week respectively. Due to higher thermal capacity of water as compared to R245fa, the rise in HTF temperature across PCM storage tank for DSOS is observed to be 7.4 times higher than ISOS. Moreover, Temperature of the PCM also increases along the length of PCM storage tank. However, relative increment in PCM temperature with respect HTF decreases with increase in length of PCM storage tank.

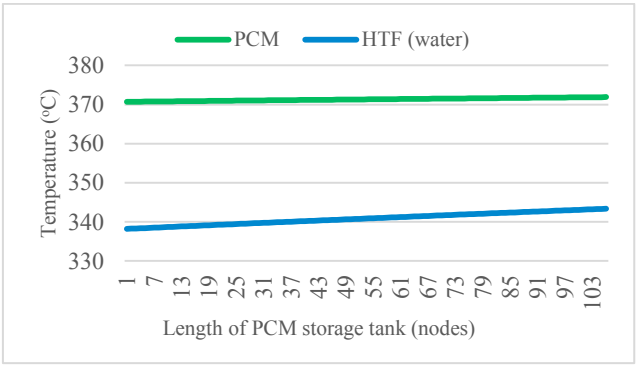

Figure 5. PCM and HTF temperature for ISOS

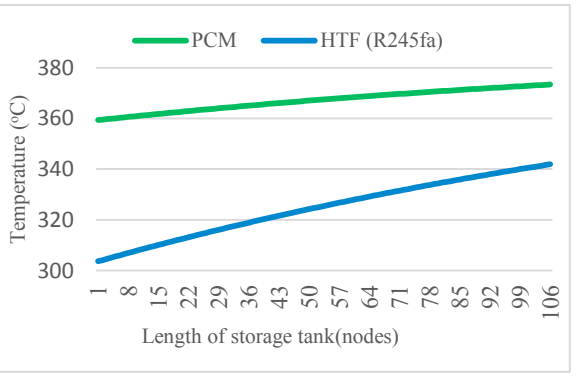

Figure 6. PCM and HTF temperature for DSOS

2.1.3. Overall system efficiencies and power output

Figure 7 shows hourly average daily system efficiency and net power of ISOS and DSOS during hottest week. DSOS has shown higher 5 times overall system efficiency and 2.4 times larger net power output as compared to ISOS on daily average basis. Both systems have shown highest efficiency and maximum power output at time 15:00 because PCM storage is charged to maximum value till that time as shown in figure 3 and 4. DSOS has shown 7.5 % higher efficiency and able to provide 6.5 kW more net power than that of ISOS on daily average basis. No of working hours for ISOS and DSOS are observed to be 12 and 13 hours, respectively. Therefore, DSOS has shown higher thermal performance as compared to ISOS. Reason behind this phenomenon is that higher thermal losses occur across ISOS and extra power is consumed to operate the solar pump.

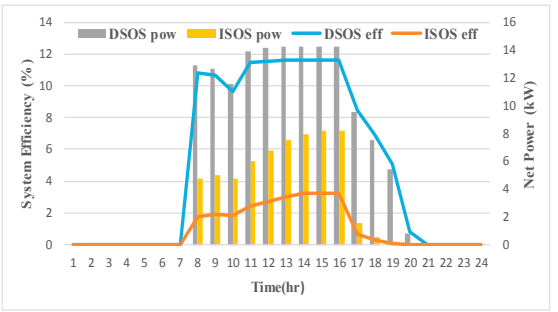

Figure 7. Overall system efficiency and net power

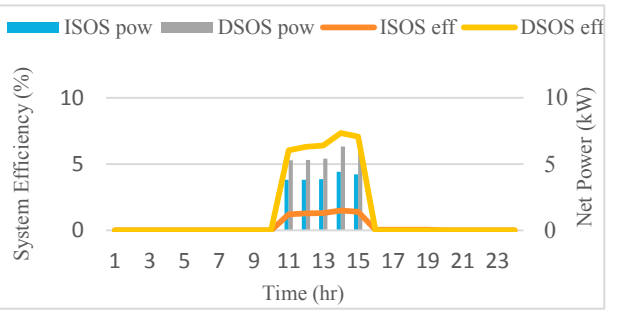

Figure 8. Overall system efficiency and net power

2.2. Performance during coldest week of the year

2.2.1. Overall system efficiencies and power output

Hourly average daily net power out and overall system efficiency of ISOS and DSOS for coldest week of the year (1st week of January) is shown in figure 8. During coldest week solar radiations and ambient temperature are very low. Therefore, HTF temperature at the inlet of PCM cannot reach the designed value of 370K. Hence, both systems does not go to charging mode. No of working hours for both systems reduces to 5. However, both of systems have shown similar behavior as in case of hottest week. DSOS has shown higher 4.5 times overall system efficiency and 1.4 times larger net power output as compared to ISOS on daily average basis. Moreover, DSOS has shown 1.09 % higher efficiency and able to provide 0.32 kW more net power than that of ISOS on daily average basis.

2.3. Performance during every month of the year

2.3.1. Overall system efficiencies & power output and energy stored during charging mode

Monthly average yearly net power out and overall system efficiency of ISOS and DSOS is shown in figure 9. Both systems have shown quiet similar behaviour as in case of weekly simulation. Figure 10 shows monthly average yearly amount of energy stored by PCM during charging mode. Amount of energy is stored in increases with increasing solar radiations and ambient temperature. Both systems have shown almost linear increment and decrement in amount of energy stored with increase and decrease in solar radiations and ambient temperature. However, ISOS has shown higher amount of energy stored as compared to DSOS.

Figure 9. Overall system efficiency and net power

Figure 10. Amount of energy strode during charging mode

2.3.2. Power Transferred to HTF during discharging and Increment in capacity factor

Figure 11 shows monthly average yearly amount of power transferred to the HTF by PCM during discharging mode. Amount of power transferred to HTF increases with increasing solar radiations and ambient temperature. Both systems have shown almost linear increment and decrement in amount power transferred to HTF with increase and decrease in solar radiations and ambient temperature. However, DSOS has shown higher amount of power transfer to HTF as compared to ISOS. Figure 12 shows monthly average yearly increment in capacity factor by use of PCM storage for both systems. Generally, increment in capacity factor increases with increasing solar radiations. However, in case of DSOS, it has shown higher increment for the months having higher solar radiations but low ambient temperature. Moreover, DSOS has shown higher increment in capacity factor as compared to ISOS.

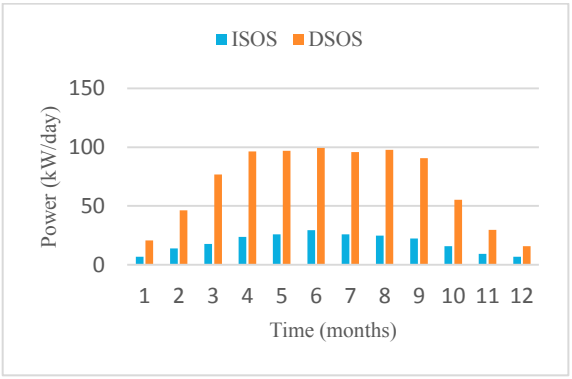

Figure 11. Power transferred to HTF during discharging

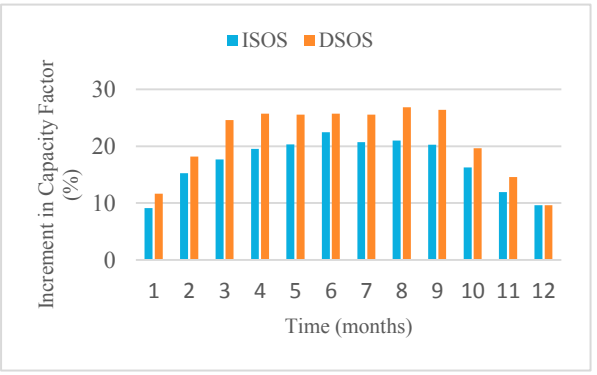

Figure 12. Increment in capacity factor

3. Conclusions

Thermodynamic comparison of ISOS and DSOS is done. DSOS has shown higher thermal performance as compared to ISOS. Although amount of energy stored is higher for ISOS but increment in capacity factor is more for DSOS because of higher thermal losses in ISOS.

4. References

[1] Hajabdollahi H, Ganjehkaviri A, Mohd Jaafar MN. Thermo-economic optimization of RSORC (regenerative solar organic Rankine cycle) considering hourly analysis. Energy 2015;87:361–8. doi:10.1016/j.energy.2015.04.113.
[2] Freeman J, Hellgardt K, Markides CN. An assessment of solar-powered organic Rankine cycle systems for combined heating and power in UK domestic applications. Appl Energy 2015;138:605–20. doi:10.1016/j.apenergy.2014.10.035.
[3] Manfrida G, Secchi R, Stańczyk K. Modelling and simulation of phase change material latent heat storages applied to a solar-powered Organic Rankine Cycle. Appl Energy 2016;179:378–88. doi:10.1016/j.apenergy.2016.06.135.
[4] Zivkovic B, Fujii I. An analysis of isothermal phase change of phase change material within rectangular and cylindrical containers. Sol Energy 2001;70:51–61.
[5] Li J, Alvi JZ, Pei G, Ji J, Li P, Fu H. Effect of working fluids on the performance of a novel direct vapor generation solar organic Rankine cycle system. Appl Therm Eng 2016;98:786–97. doi:10.1016/j.applthermaleng.2015.12.146.
[6] Meteonorm. Global Solar Radiation Database - METEONORM 2015.